

Annealing Behavior of Gel-Spun Polyethylene Fibers at Temperatures Lower than Needed for Significant Shrinkage

WENBING HU,^{1,2} ALEXANDER BUZIN,^{1,2} JAR-SHYONG LIN,³ BERNHARD WUNDERLICH^{1,2}

¹Department of Chemistry, University of Tennessee, Knoxville, Tennessee 37996-1600

²Chemical and Analytical Sciences Division, Oak Ridge National Laboratory, Oak Ridge, Tennessee 37831-6197

³Solid State Division, Oak Ridge National Laboratory, Oak Ridge, Tennessee 37831-6377

Received 23 April 2001; revised 15 August 2002; accepted 19 September 2002

ABSTRACT: The annealing at 373 K of ultrastrong, gel-spun polyethylene (PE) has been studied. At this temperature, the fibers show no significant shrinkage. Still, a significant decrease in the mechanical properties is observed. The fibers have been analyzed with differential scanning calorimetry (DSC), temperature-modulated differential scanning calorimetry (TMDSC), atomic force microscopy (AFM), and small-angle X-ray scattering (SAXS). During the annealing, the glass transition of the intermediate phase is exceeded, as shown by DSC. When split for structure analysis by AFM, the annealed fibers undergo plastic deformation around the base fibrils instead of brittle fracture. The quasi-isothermal TMDSC experiments are compared to the minor structural changes seen with SAXS and AFM. The loss of performance of the PE fibers at 373 K is suggested to be caused by the oriented intermediate phase, and not by major changes in the structure or morphology. The overall metastable, semicrystalline structure is shown by TMDSC to possess local regions that can melt reversibly. © 2003 Wiley Periodicals, Inc. *J Polym Sci Part B: Polym Phys* 41: 403–417, 2003

Keywords: gel-spun polyethylene fibers; annealing; differential scanning calorimetry (DSC); atomic force microscopy (AFM); temperature-modulated differential scanning calorimetry (TMDSC); SAXS; structural changes; properties

INTRODUCTION

Gel-spun, ultrastrong polyethylene (PE) fibers of ultrahigh molar mass have a better performance ratio of mechanical properties and damage tolerance than aromatic fibers,¹ but this advantage is limited to temperatures below 373 K,² although significant shrinkage along the fiber direction occurs only above 400 K,³ closer to the onset of melting. Therefore, a study of these fibers before

significant shrinkage, as described in this article, is of interest.

The structure of gel-spun, ultrastrong PE fibers has been analyzed previously with many techniques. The model of conventional fibers may still be used for this analysis; that is, there are sheaves of macrofibrils greater than 50 nm in width that, in turn, consist of microfibrillar structures approximately 5 nm wide.⁴ The lamellar structure has disappeared on ultradrawing, as shown by transmission electron microscopy (TEM),⁵ IR spectroscopy, and small-angle X-ray scattering (SAXS).⁶ A memory of the predrawn structure is obvious because on annealing at a high temperature, shrinkage causes a change in

Correspondence to: B. Wunderlich (E-mail: wunderlich@chartertn.net)

Journal of Polymer Science: Part B: Polymer Physics, Vol. 41, 403–417 (2003)
© 2003 Wiley Periodicals, Inc. *This article is a US Government work and, as such, is in the public domain in the United States of America.

shape toward the original shape. In fact, longitudinal shrinkage and lateral expansion are the cause of many erroneous results in differential scanning calorimetry (DSC). A simple tight enclosure of a fiber in a crimped aluminum pan will restrict the expansion and lead to partial or full constraint in experiments in which conditions of free shrinkage are intended.⁷ More recently, this influence of the initial morphology was proven by transverse TEM on a micrometer scale of resolution.^{8–10}

Raman spectroscopy of ultrastrong PE fibers revealed two types of strain in the trans-conformation of extended chains, which went parallel to the splitting of the 002 fiber-diffraction peak seen by wide-angle X-ray scattering.^{11–13} The noncrystalline, highly strained chains were attributed to taut tie molecules and were later called an oriented intermediate phase with a mobility between that of amorphous and crystalline PE, as measured by solid-state ¹³C NMR.^{14–16} For commercial, gel-spun PE (Spectra 2000), the oriented intermediate phase can amount to as much as 33%.¹⁶ A model of the fibers requiring at least three phases was suggested for such gel-spun fibers, namely, crystalline, amorphous, and oriented intermediate phases.¹⁷ Solid-state-extruded and high-temperature-ultradrawn fibers are assumed to be similar in structure to the gel-spun fibers of this research. The sizes of crystallites and voids within such fibers reach beyond 100 nm; that is, they form macrofibrils. The size of the oriented chains connecting the crystallites along the fiber direction is only about 10 nm.¹⁸ In addition, small amounts of the monoclinic crystalline phase have been found in ultrastrong PE fibers.¹⁹ The formation of monoclinic crystals is a general property of semicrystalline PE stressed beyond the yield point.²⁰ The quantity of monoclinic crystallites in gel-spun PE can be increased by lateral compression.^{17,21} The internal structure of the ultrastrong fibers has been revealed by electron microscopy after permanganic acid etching of the surface.⁸ In transverse sections, cratering is visible, and in longitudinal sections, extended, density-deficient regions between the macrofibrils can be seen. With solid-state NMR, it was found that with heating from 295 to 413 K, 40 K above the analyzed annealing temperature used here, only small decreases in the mass fraction of the orthorhombic phase could be observed, and the oriented intermediate phase increased, whereas any monoclinic phase disappeared before 373 K was reached.²² Electron microscopy on con-

ventional PE fibers with a low draw ratio of 11 recrystallize on annealing at 393 K on the surface of ribbon-shaped macrofibrils into a network of lamellar crystallites.²³ Similarly, fibers drawn out of extended-chain crystals recrystallize into a shish-kebab morphology with 3 min of annealing at 393 K.²⁴ In this article, we show that annealing at 373 K does not cause such morphology changes. Instead, it leaves the metastable, orthorhombic crystal network largely intact but relaxes some of the strain in the intermediate phase between the crystals.

More attention has been focused on the melting of gel-spun PE fibers than on low-temperature annealing. On heating, the X-ray diffraction pattern of the orthorhombic phase disappears at about 433 K.^{7,25} If the fibers are longitudinally or laterally constrained, a hexagonal mesophase appears in the melting range, as found by X-ray diffraction^{7,19,26} and solid-state ¹³C NMR.²⁷ The mesophase has been identified as a conformationally disordered structure (CONDIS crystal)²⁸ by X-ray diffraction and IR/Raman spectroscopy.²⁹ Calorimetry indicates a heat of transition of this intermediate phase on isotropization.⁷ Multiple melting peaks occur in constrained samples on DSC.^{30–32} Without constraint, less complicated and even single melting peaks can be observed.^{7,32,33} Three melting peaks have been identified with the help of X-ray diffraction.^{19,34} The first peak is usually found between 413 and 421 K and corresponds to the melting of crystallites with sufficient constraints to raise the observed melting temperature up to and beyond the equilibrium. Macroscopic extended chains have an equilibrium melting temperature of 414.6 K.^{35,36} The second peak, located between 422 and 428 K, is thought to have a contribution from the orthorhombic-to-hexagonal phase transition of highly constrained crystallites. The third peak is located at about 433 K and is thought to be caused mainly by the melting of the hexagonal crystallites and accompanied by extensive longitudinal shrinkage and transverse expansion. A parallel spine structure along the fiber direction has been observed, which can survive for a long time under constraint at 426 K.³⁷ The spines are possibly an indication of remnants of the initial fiber structure, sustained by the constraint.

In this article, we focus on the annealing behavior at 373 K, a temperature lower than needed for significant shrinkage and melting, but at this temperature the yield stress has already begun to decrease rapidly, and the stress–strain behavior

has changed from brittle to ductile.³⁸ A thermal analysis must consider the fact that the glass transition of the rigid amorphous fraction is completed at this temperature (it ranges up to 300 K), and the upturn of the apparent heat capacity beyond the vibrational heat capacity due to beginning fusion starts at about 375 K.⁷ Therefore, at 373 K, the orthorhombic crystallites remain metastable with limited mobility of the chains along the chain axis (sliding diffusion³⁹), whereas the amorphous phase and the intermediate phase (CONDIS crystal²⁸) have their respective conformational mobilities.

EXPERIMENTAL

Sample Description

The sample used in this research was a commercially available gel-spun, hot-stretched Spectra 900 fiber with a molar mass greater than 10⁶ Da, produced by Allied-Signal, Inc. Detailed information about this specific sample was available from Allied-Signal (Young's modulus = 125 GPa, tensile strength = 2.7 GPa)³ and, in addition, was generated in previous publications from our laboratory (sample PEIII, density = 0.974, crystallinity from density = 86%, crystallinity from calorimetry = 92%).^{7,16,17,32}

DSC and Temperature-Modulated Differential Scanning Calorimetry (TMDSC) Measurements

The standard DSC measurements were performed with a PerkinElmer Pyris-1 DSC instrument with a CryoFill liquid-nitrogen cooler. The temperature scale of the calorimeter was calibrated at the onset of the melting of ice (273.15 K), indium (429.75 K), and tin (505.03 K). A preliminary calibration of the heat-flow rate was set with the heat of fusion of indium (28.45 J g⁻¹) at a scanning rate of 10 K min⁻¹. The purge gas was pure helium, moving at a flow rate of 25 mL min⁻¹. The heat capacity measurements were performed in the DDSC mode, which is based on a sawtooth modulation of temperature. Three parallel runs were performed, all with the same empty pan in the reference side of the twin calorimeter. On the sample side, one run was made with an empty pan; the next was made with the sample enclosed in an empty pan of the same weight; and the last run was made with a reference material enclosed, again, in a pan of the

same weight as used for the sample run and placed on the reference side. The first run established the asymmetry of the calorimeter and fixed the zero line for the subsequent runs, the second was used for the actual measurement, and the last run enabled the point-to-point calibration. The reference material was sapphire (Al₂O₃) in a flat, single-crystalline disk (26.026 mg) of a well-known heat capacity.⁴⁰

The reversing heat capacity, c_p , is calculated as follows. The standard DSC responses of the heating and cooling segments of each modulation cycle are evaluated after they have reached the steady state (Φ_h and Φ_c , respectively, after baseline correction). Similarly, the steady-state rates of the change of temperature are established at the end of their programmed heating and cooling segments (q_h and q_c , respectively). The evaluation is done without Fourier transformation, with the following equation:⁴¹

$$mc_p = \frac{\Phi_h - \Phi_c}{q_h - q_c}$$

where m is the sample mass. This method of evaluation of data after the steady state is reached keeps the advantage of standard DSC and allows the evaluation of reversing processes. In case the chosen period, p , is too short to reach the steady state, that is, the calorimeter does not attain a heat-flow rate that is practically parallel to the baseline, p must be extended, or a quasi-isothermal analysis method must be used, as described later. Furthermore, this method also permits us to compute the irreversible contribution to the heat capacity from the difference of the apparent heat capacities at the ends of the heating and cooling segments without transferring the errors originating from the reversing heat capacity computed from a flawed Fourier analysis to the nonreversing heat capacity.

A sample of 6–12 mg was rolled tightly on a thin rod, slid off the rod into the pan as a mat, and tightly crimped with the lid. The sample is, therefore, under constraint with respect to lateral expansion, and significant shrinkage along the fiber direction is also inhibited when lateral expansion is impeded.⁷ All samples and pans were weighed with a CAHN-28 electrobalance.

Atomic Force Microscopy (AFM) Observations

The AFM images were obtained with a Digital Instruments Nanoscope IIIa, with standard pyra-

midial Si_3N_4 nanoprobes, mounted on a cantilever with a spring constant of 0.06 N m^{-1} . All scanning was done in air at ambient temperature. The tip motion was monitored by a laser beam. Images were collected in the contact mode (constant-force mode) within a $15\text{-}\mu\text{m}$ scanning range. So that the sample would not move during scanning, it was mounted on a metal substrate with a piece of double-stick tape. The positioning of the tip on the surface of the sample was possible with the built-in optical microscopic stage. The forces necessary to obtain stable images were adjusted, depending on the scanning rate and the range of the local surface topography. The forces were minimized to obtain better clarity of the images. The scanning rate was $0.5\text{--}3 \text{ Hz}$, depending on the size of the images. All the AFM images were flattened by subtraction of the first-order level of the average plane without further mathematical treatment for contrast enhancement.

The internal morphology can be better assessed by the splitting of the fibers before AFM. The exposed surfaces reveal characteristic internal structures. The Spectra 900 fiber was split along the fiber direction as follows. First, a segment of the fiber was cut to a length of about 10 mm and mounted for half of its length on double-stick tape, previously fixed on the support stage. The free end of the fiber was then abraded with a knife-edge until fibrillation occurred. Second, the fibrillated fibers were gathered into two parts, and each part was gripped with tweezers and split along the fiber into the mounted segment. Third, both the split and unsplit surfaces were mounted for observation. The endpoint of the splitting could be found with the optical microscope.

Fibers of a length of about 100 mm were annealed in an oven at $373 \pm 3 \text{ K}$ for the indicated times and also split after cooling for the AFM observations. The shrinkage on annealing was measured by a ruler with a 1.0-mm graduation.

SAXS Measurements

The SAXS measurements were made at the ORNL 10-m SAXS facility with a rotating anode X-ray source ($\text{Cu K}\alpha$, wavelength $\lambda = 0.154 \text{ nm}$), pinhole collimation with a 2-mm diameter at the sample, and a two-dimensional, position-sensitive detector. The scattering angle (θ) range was determined by the adjustment of the sample-to-detector distance: the 5-m configuration permitted a $0.08\text{--}0.8\text{-nm}^{-1}$ scattering momentum transfer Q

$[(4\pi/\lambda) \sin(\theta/2)]$, and the 2-m configuration corresponded to a Q range of $0.1\text{--}2.0 \text{ nm}^{-1}$. The size of the scattering object was approximated by $2\pi/Q$. The reported scattering intensities were corrected for instrumental background, dark current due to cosmic radiation, electronic noise in the detector circuitry, and detector nonuniformity and efficiency on a cell-by-cell basis.⁴²

The fiber was tightly wound on a square aluminum frame with a lateral size of about 15 mm and a thickness of about 2 mm. The frame was then mounted onto the sample holder, and the X-ray beam passed through the sample in the hollow of the central part of the frame.

RESULTS

DSC Measurements

The effect of annealing at 373 K on the subsequent melting peaks was first evaluated by standard DSC measurements. The original fibers were heated from 293 to 453 K at a rate of 40 K min^{-1} . Figure 1 shows the expected three peaks for the constrained fibers (top curve). For the other two samples, the scanning was interrupted at 373 K for 5 and 30 min for annealing before the runs were completed (dashed and dotted curves of Fig. 1). After annealing, the heat-flow-rate curves show small changes in the amplitudes of the melting peaks. The peak heights were estimated from a baseline extrapolated from the melt. The results are listed in Figure 1. With annealing time, the first peak height increases, the second changes little, and the third decreases. Annealing effects were also seen when variable scanning rates were used, as was already described earlier.^{17,19}

Figure 2(a) reveals something of the nature of the three melting peaks. The experiment involved interrupting the DSC experiment between the first and second melting peaks. The original fiber was heated to 424 K (curve 1), cooled (curve 2), heated again to the melt (curve 3), and finally cooled from the melt (curve 4). All heating and cooling runs were made at the same rate of 10 K min^{-1} .

Surprisingly, during cooling in curve 2, a small exotherm is seen at about 415 K. Major crystallization occurs at about 410 K, which is still much higher than the temperature observed for crystallization from the relaxed melt when seeded with extended-chain crystals. After 15 min of isothermal crystallization, the first crystals were seen at

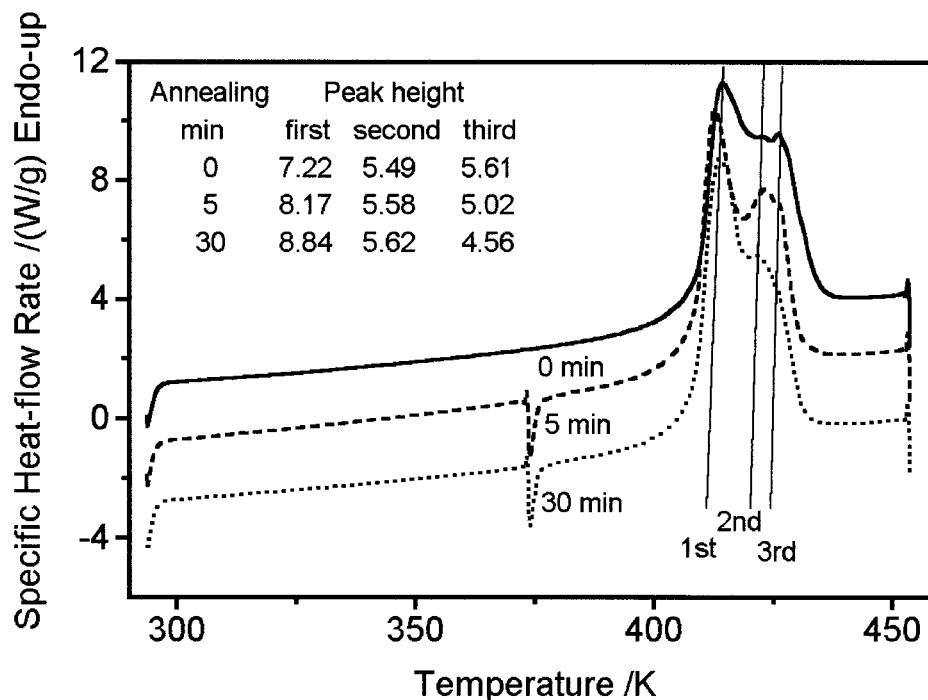


Figure 1. Curves of the specific heat-flow rate by standard DSC before and after annealing at 373 K for 5.0 and 30 min. The scanning rate was 40 K min⁻¹. The sequence of the melting peaks is designated by the straight lines. The peak heights over the liquid baseline are listed.

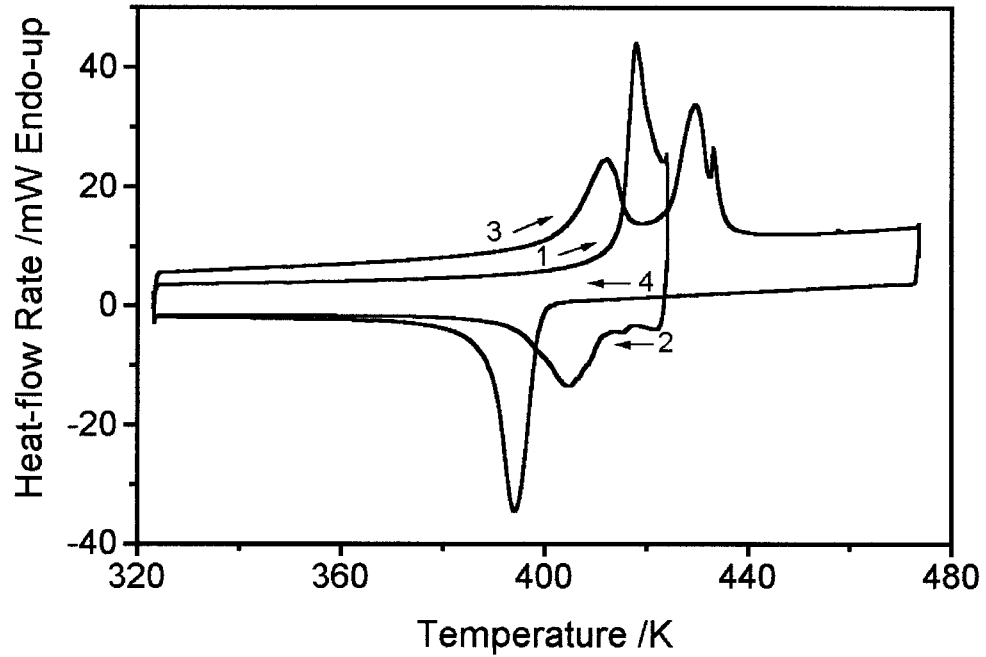
approximately 400.5 K.⁴³ The first melting peak in curve 3 is broader than that in curve 1 and is shifted to a lower temperature. The second and third peaks are still prominent in curve 3. After the heating to 473 K, the cooling curve 4 shows crystallization at approximately 400 K, lower than in curve 2, at a temperature similar to that quoted for the relaxed melt.⁴³ On subsequent reheating, a larger single melting peak was found.

Figure 2(b) displays the heating of the original fiber to 433 K, a temperature located between the second and third melting peaks (see curve 1). The analysis goes parallel to Figure 2(a). Major crystallization on cooling is seen in curve 2, again starting at approximately 410 K, with a small exotherm remaining at 415 K. These small exotherms in Figure 2(a,b) at about 415 K could not be identified but may be a reordering of the hexagonal-to-orthorhombic phase transition due to the reduced residual strain. The first melting peak on reheating (curve 3) is lowered, as before, but indicates now a much larger latent heat. Only a small fraction of the second peak remains, without indication of a third peak. After heating to 473 K and cooling, curve 4 is the same as in Figure 2(a).

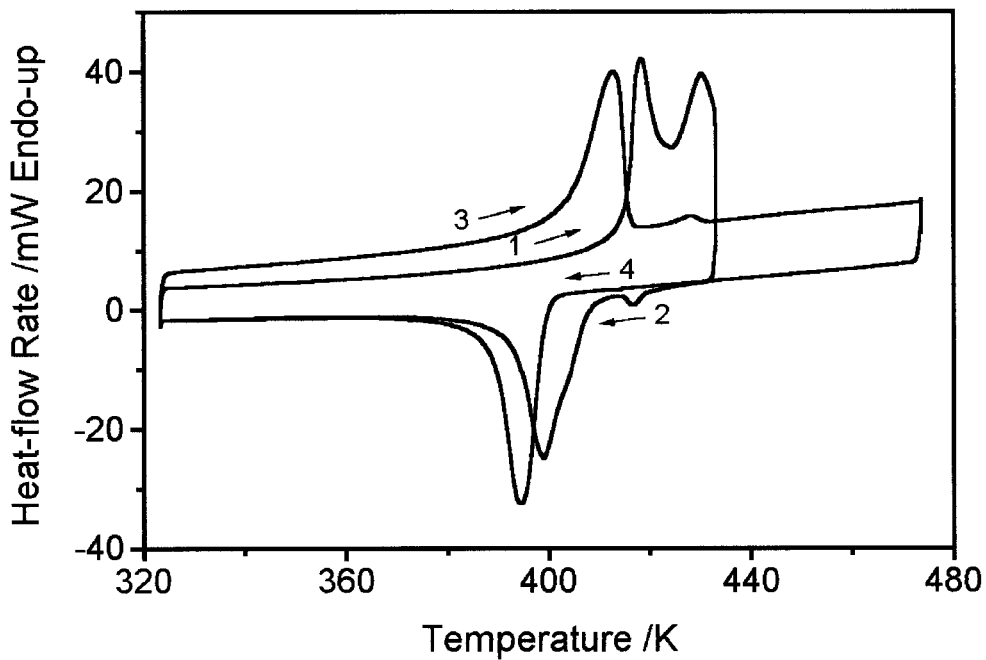
A comparison of Figure 2(a,b) clearly demonstrates that the first and second melting peaks are caused by crystallites in differently strained environments, and the third peak is contiguous with the occurrence of the second peak. Stopping the heating at 433 K relieves so much of the constraint that no hexagonal crystals are formed on reheating [curve 3, Fig. 2(b)].

These observations are in agreement with this identification of the three endotherms.^{7,37} The single endotherm observed when the fibers are heated without lateral and longitudinal restraint^{7,32,33} is the result of a continuous, concerted strain relaxation and melting during the collapse of the global structure of orthorhombic crystals.

A quantitative separation of the three peaks seen in Figure 1 is not possible because of their overlap and the unknown shapes for each transition. Qualitatively, Figure 2(a) shows that many of the crystals with an elevated melting temperature due to the attached strained noncrystalline molecules remain after quenching from 424 K, as judged from the enhanced crystallization temperature and the shape of the endotherm of curve 3. From the sizes of the endotherms in curve 3, it is



(a)



(b)

Figure 2. (a) Curves of the heat-flow rate by standard DSC (1) on heating beyond the first melting peak to 424 K, followed by (2) cooling, (3) reheating, and (4) final cooling from the melt starting at 473 K, and (b) curves of the heat-flow rate by standard DSC (1) on heating beyond the second melting peak to 433 K, followed by (2) cooling, (3) reheating, and (4) final cooling from the melt starting at 473 K.

clear that only a small portion of the crystals in peak 2 ends up contributing to the peak 3 because the heat of fusion of the hexagonal PE has been estimated to be about half that of the heat of fusion of orthorhombic PE, which leaves the other half for the orthorhombic-to-hexagonal transition.^{19,28} Also, it must be remembered that under atmospheric pressure, the hexagonal phase is not stable at any temperature; that is, as soon as the strain from drawing is relaxed, the melting of all crystals must commence as soon as the zero-entropy-production melting temperature is exceeded.

TMDSC Measurements

The reversing heat-flow rate was measured at an underlying heating rate of 1.0 K min^{-1} with scanning at a heating rate of 4.0 K min^{-1} for 0.5 min, followed by cooling at 2.0 K min^{-1} for another 0.5 min. The reversing heat capacity was calculated with eq 1 and gave reliable data as long as the steady state was reached after 0.5 min. Figure 3(a) illustrates the apparent heat capacities of the fiber on the first and second heating in the temperature region before significant melting occurs. The first heating was carried out from 213 to 453 K, far into the melt. After the first run, the sample was cooled at a rate of 10 K min^{-1} and followed by the second heating run. The second scan, therefore, represents a sample crystallized from the melt without drawing. The somewhat higher heat capacity in the second scan implies a larger amorphous content. The melting and reorganization begin at a lower temperature than in the first scan. The heat capacities of the original fiber in the first scan agree well with the previously reported data.⁷ In this temperature region, each heating and cooling segment has reached the steady state. With respect to the recommended amorphous and crystalline PE data of the ATHAS (Advanced Thermal Analysis System) data bank,⁴⁴ the apparent heat capacity of the original fiber starts to deviate from the fully crystalline data with a broad glass transition and crosses the amorphous heat capacity at 378 K.

In Figure 3(b), the data of Figure 3(a) are continued into the melting range. Additional quasi-isothermal TMDSC measurements were taken with a modulation amplitude of 1.0 K because of the inability of the sample in the melting range to reach the steady state within 0.5 min. In the quasiisothermal measurements, the heat capacities were calculated from the last period of each run, again with eq 1 at the indicated temperature,

T_0 . In the first scan, the annealing of the original fiber caused by the quasi-isothermal waiting times at a lower temperature does not change the apparent reversing heat capacity up to 405 K. After the glass transition and some increase in the heat capacity due to the change in the gauche–trans equilibrium within the crystal, that is, between 375 and 405 K, there is a considerable contribution of reversible latent heat [see also Figs. 3(a) and 10 in an earlier work⁷]. This result is further confirmed by the negligible change in the apparent reversible heat capacity, which is noted after a quasi-isothermal measurement at 400 K and a return to 395 K for a second measurement for 30 min (indicated by the curved arrow). With the second heating, the TMDSC data above 360 K are higher than the quasi-isothermal data, indicating an increasing amount of annealing before a reversible process. We conclude that annealing at 373 K does not significantly change the reversible heat capacity, nor is there substantial melting, recrystallization, or crystal perfection that would cause irreversible endotherms or exotherms.

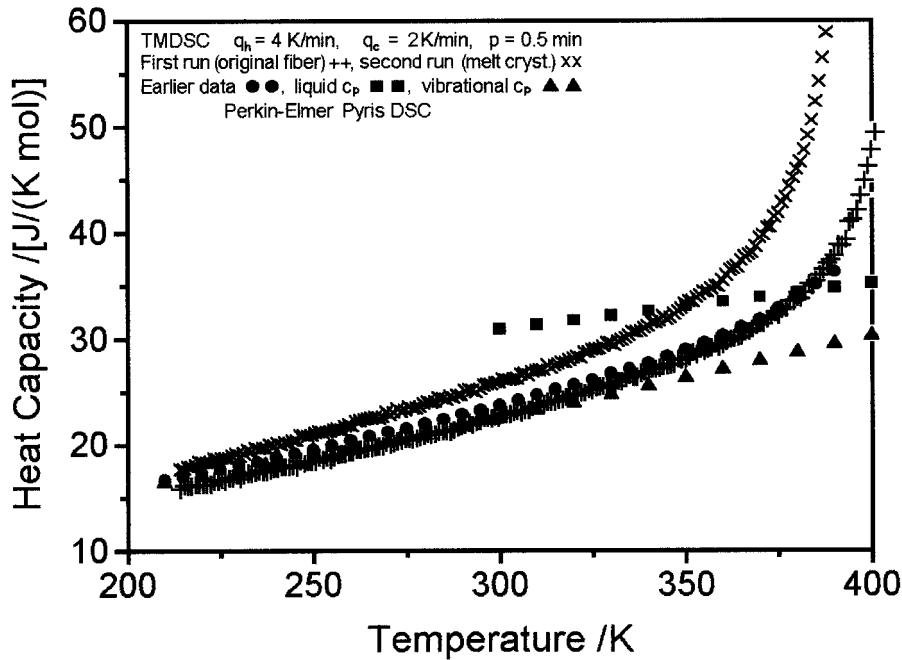
If the original fiber is heated directly to 415 K without a stop at lower temperatures, at a heating rate of 200 K min^{-1} , the quasi-isothermal measurement shows a higher apparent reversing heat capacity, even though the sample was annealed at this temperature for 120 min before the measurement. At this temperature, at which the less constrained crystallites have melted, the apparent reversing heat capacity clearly depends on previous annealing effects below this temperature. The shorter the annealing time is, the larger the apparent reversing heat capacity is. This annealing starts only at about 405 K, as can be judged from the difference between the TMDSC and quasi-isothermal TMDSC data. Furthermore, at 420 K, the heat capacity of the melt is reached after about 40 min of modulation. There is no indication of reversing melting in the quasi-isothermal data above 415 K, at which the positions of the second and third melting peaks are located in Figure 1. At this temperature, the sample is fully melted.

Observations by AFM

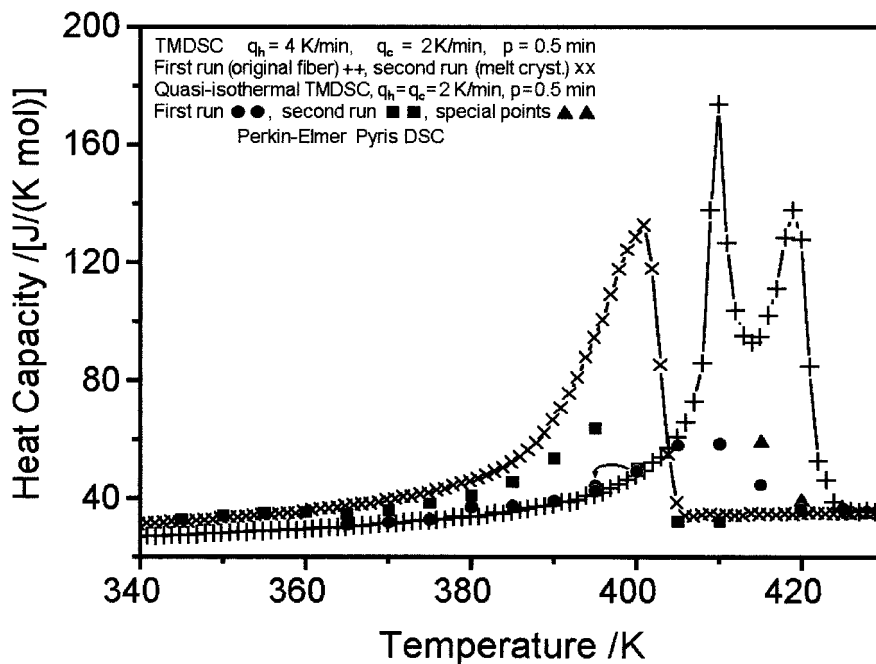
Figure 4(a) illustrates the outside surface of the original fiber. The macrofibrils have a width of 100–200 nm. In Figure 4(b), a split surface of the original fiber is shown. It is a rough fracture surface; the grooves in the surface have a width of

50–200 nm and run parallel to the fiber direction. This implies that the overall fibers consist of macrofibrils surrounded by a weaker matrix. Defects are expected along the direction of the fiber.^{19,45} The kink band in Figure 4(b) looks similar to those seen when extended-chain crystals and

highly oriented semicrystalline and amorphous fibers are fractured.⁴⁶ Figure 4(c) illustrates a split surface of a fiber exposed to hot air (373 K) for 30 min. The roughness due to the splitting seems to soften, but the macrofibrils can still be made out, and an even finer structure appears,



(a)



(b)

perhaps indicating the bundles of microfibrils. The kink band shows an accumulation of sharper fibrils that, on further magnification, seem to be covered with transverse lamellae. The results shown in Figure 4(c) are similar to those of epitaxial recrystallization observed on surfaces of fibrils on annealing.²⁶

If the original fiber is annealed in hot air at 373 K for a time longer than 5 min, its surface changes little from that seen in Figure 4(a), but the surface produced by splitting has a much different appearance than that seen in Figure 4(b,c). Figure 5 reveals a smooth band structure on the split surface. The shrinkage along the fiber direction during this annealing is still less than 1%. Annealing for longer times enhances this structural change, and wider band structures can be observed. The cross-sectional heights are about 100 nm, close to the transverse size of the macrofibrils of Figure 4. Some macrofibrils can be recognized on the smooth surface of the band structure and may offer a link to the history of the generation of the new structure. The thin striations running perpendicular to the expected chain direction on the smooth surface have also been observed on the surface of extended-chain crystals of PE on brittle fracture⁴⁷ and can be attributed to the shock waves generated during the splitting of the fibers. The band structure with its smooth surface can still be observed when the splitting is performed in liquid nitrogen or when the split surface is exposed to hot air (373 K) for 30 min.

Figure 6(a) illustrates the boundary between a smooth surface region and a rough surface region observed with the splitting of a sample after 30 min of annealing at 373 K. The morphology of the rough surface looks similar to the outside surface of the original fiber [see also

Fig. 4(a)]. The angle between the two kinds of surfaces across the horizontal, marked by the two arrows in Figure 6(a), is shown in Figure 6(b) in a cross-sectional elevation plot. The two different surfaces include an angle close to 90°. Because the original fiber has an elliptical cross section,^{3,8} the split surface should have an angle larger than 180° to the outside surface. The smaller angle between the smooth, split surface and the rough surface indicates that we are dealing with an inside surface of the fiber, which may belong to a void or a crack.

In summary, the AFM data reveal the previously described macrofibrils and microfibrils in Figure 4(a). On the splitting of the unannealed fibers, they undergo a brittle fracture with occasional kink bands [Fig. 4(b)]. On the annealing of these fracture surfaces at 373 K, only small changes are visible [Fig. 4(c)]. Similarly, the annealing of the fibers at 373 K produces few changes on the internal surfaces, as seen in Figure 6(a). The external surfaces still have an appearance similar to that before annealing [Fig. 4(a)]. On splitting, the fracture is changed locally from brittle to plastic [see Figs. 5 and 6(a)].

Measurements by SAXS

Figure 7(a,b) shows the equatorial and meridional scattering intensity curves with a sample-to-detector distance of 5 m. After annealing at 373 K, these curves show practically no changes over the whole scattering range of 8–80 nm. For $Q < 0.2 \text{ nm}^{-1}$, perhaps there is a small tendency toward a peak in the meridional curves, but the faint indication of a more regular structure in the size range of 30–60 nm is not considered definitive enough for a more detailed interpretation. In the 2-m configuration of the SAXS experiments, the

Figure 3. (a) Reversing heat capacities up to the beginning of melting. Measurements were made with sawtooth-type TMDSC with an underlying heating rate of 1 K min^{-1} for the (+) first and (×) second heating. (●) Data from a previous analysis of the same material are marked, and (▲) the calculated vibrational heat capacity data for 100% crystalline PE are indicated, as well as (■) the data for liquid PE.⁷ (b) Reversing heat capacities up to the beginning of melting. Measurements were made with sawtooth-type TMDSC with an underlying heating rate of 1 K min^{-1} for the first and second heating. These data were augmented by numerous successive quasi-isothermal TMDSC runs with data taken after 10–130 min, depending on the time needed for the steady state. The second point at 395 K, connected by a curved arrow, was a repeat taken after the 400 K point and was followed by the regular measurement at 405 K. (▲) Two points were taken directly after quick heating from room temperature to 415 K, followed by the 420 K point.

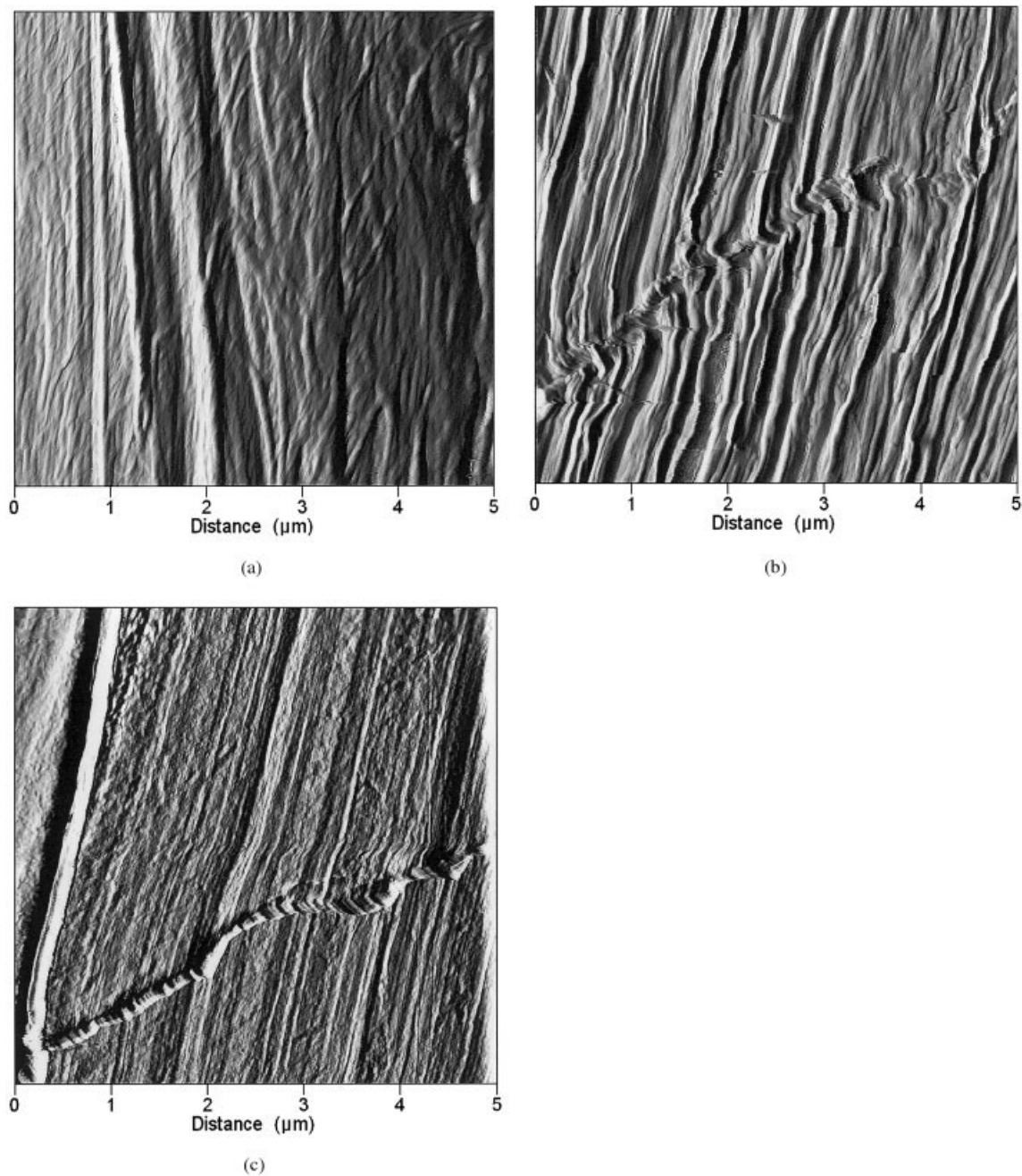


Figure 4. Images of the surfaces of the original PE fiber by AFM (the fiber directions are parallel to the macrofibrils): (a) the outside surface, imaged with a z range of 2.00 nm; (b) the surface after the splitting of the fiber, imaged with a z range of 8.00 nm; and (c) the image of a split surface, as seen in Figure 4(b), after annealing at 373 K in hot air for 30 min. The z range of the image is 10.00 nm.

lower limit of the scattering range is extended to 3 nm, but there is also no apparent change in the intensity of the scattering curves. This lower size limit has reached the size scale of the microfibrils (≈ 5 nm).

DISCUSSION

During fiber formation, polymer chains are thought to be drawn into microfibrils through a sliding motion involving crystals and intercrystal-

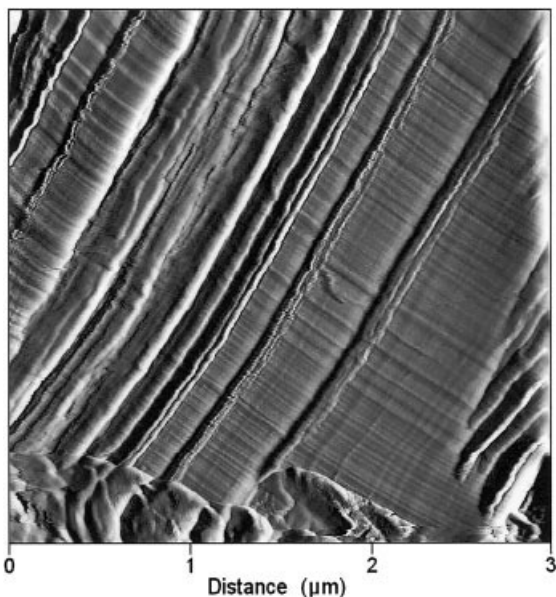


Figure 5. Image of the surface of a PE fiber by AFM, split after being annealed for 5 min at 373 K. The z range of the image is 10.00 nm. The fiber direction is parallel to the deep grooves in the surface.

line material.⁴⁸ On further deformation by ultra-drawing, the intrafibrillar and interfibrillar tie chains are sustaining the additional stress of drawing and are ultimately fixed into a metastable structure, which is supported by the more stable orthorhombic crystallites. Initially, these tie chains were described as taut tie molecules.^{14,49} Later, they were quantitatively assessed as the oriented, mobile intermediate phase, a third phase oriented with its chains in the draw direction and having a large fraction of trans conformations of a mobility intermediate between crystal and melt¹⁶ but without lateral order.¹⁷ The oriented intermediate phase was found to also have a lower enthalpy than the melt, and in gel-spun fibers of the Spectra 900 type, it is about 30% of the total mass of the fiber.⁷ On full relaxation of the oriented intermediate phase, one would, therefore, expect a heat of transition. Our TMDSC measurements have verified that the glass transition of the amorphous and intermediate phases reaches 50 K higher (to ca. 300 K) than that in a fully amorphous sample, but they do not show any significant change in the heat-flow rate or reversing heat capacity after annealing at 373 K for 30 min [see Figs. 1 and 3(b)]. This kind of transition must, if it takes place at all, be minimal. The largely parallel macrofibrils seen on the surface of the fibers by AFM in Figure 4(a) represent microfibrils dispersed in an interfibril-

lar, oriented intermediate phase, similar to an earlier suggested fiber structure model.⁵⁰ On the splitting of the fibers, a unique, grooved surface with kink bands results, as seen in Figure 4(b). Kink bands form commonly on compressive deformation and may, therefore, have been introduced during the splitting. The grooving on a scale of the macrofibrils can be interpreted by analogy to the extended-chain crystals:⁵¹ the element around which the fracture path proceeds is the macrofibril instead of the molecular chain. Surrounding each macrofibril, one expects the oriented intermediate phase, which permits easier fracture propagation without destruction of the more rigid orthorhombic crystallites and the basic macrofibrillar morphology. The annealing of the split surface at 373 K causes, as seen in Figure 4(c), a certain amount of softening and smoothing that reveal a somewhat smaller structure, and in places of larger deformation, such as on the kink bands, the annealing takes the form of epitaxial recrystallization,²³ as also seen on fracture surfaces of extended chain crystals.²⁴ In Figure 4(c), the individual macrofibrils lose their smooth surface, most likely by an improvement in the cover layer, similar to the earlier suggested “slackening of the taut tie molecules.”⁵² The annealing of the surface seems to involve only the oriented intermediate phase.

The SAXS results in Figure 7(a) indicate that there is not enough regularity in the lateral sizes to yield scattering maxima, and no changes occur on annealing. Figure 7(b) also shows no longitudinal regularity, although during annealing a small change in the length scale may occur between 30 and 60 nm. The SAXS curves taken in the 5-m and 2-m configuration indicate no presence before annealing, or formation on annealing, of regularly chain-folded crystals with a thickness down to at least 5 nm; that is, the possible folded-chain crystals in the kink bands of the AFM picture in Figure 5(c) are not a widespread phenomenon within the fiber. There may not be enough space or mobility for the slackened chains to re-fold. In fact, the rather featureless increase of the diffraction intensity at low values of Q has been explained as originating from large voids⁵³ and the shapes of the crystallites.⁵⁴ Overall, one must conclude that the structure analysis has proven that no significant changes occur during the annealing. The observed major difference is that after annealing, the splitting of the fibers that led to brittle fracture around the macrofibrils has changed to plastic deformation of the oriented intermediate phase.

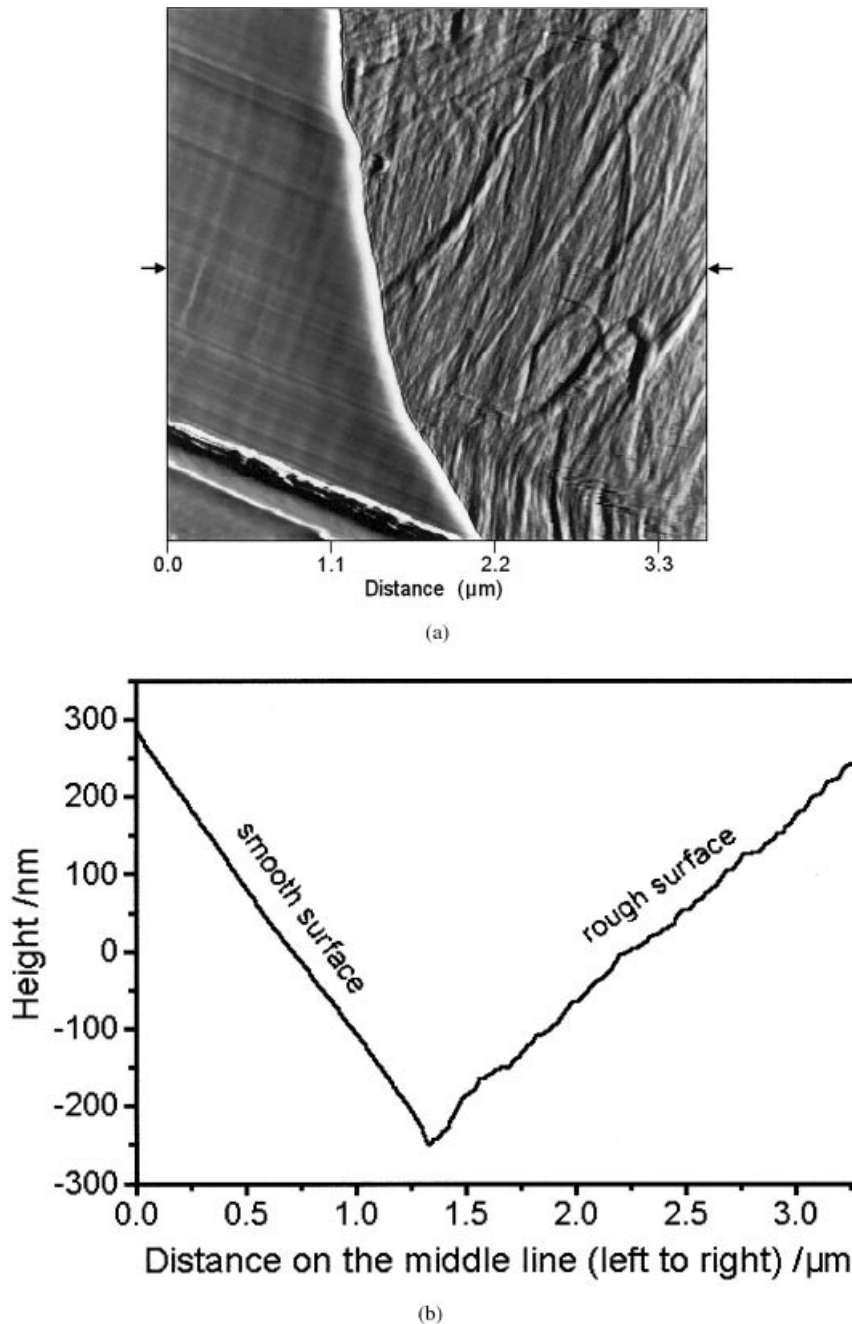


Figure 6. (a) Image of the surface of a PE fiber by AFM, split after being annealed for 30 min at 373 K. The z range of the image is 10.00 nm. The fiber direction is parallel to the macrofibrils on the rough surface portion. The arrows indicate the direction along which (b) the cross-sectional height analysis was performed.

Calorimetry is a macroscopic technique that probes the state of molecular motion through heat capacity and allows insight into phase transitions through the measurement of latent heats. The DSC and TMDSC experiments were undertaken to elucidate possible minor changes in the motion and phase distribution within the fibers. The DSC

trace on the heating of the initial fibers in Figure 1 illustrates the typical behavior of gel-spun, high molar mass PE when analyzed under external constraints before and after annealing at 373 K. Most melting occurs in all cases above the equilibrium melting temperature of PE.^{7,55} This increased melting temperature is caused by the mo-

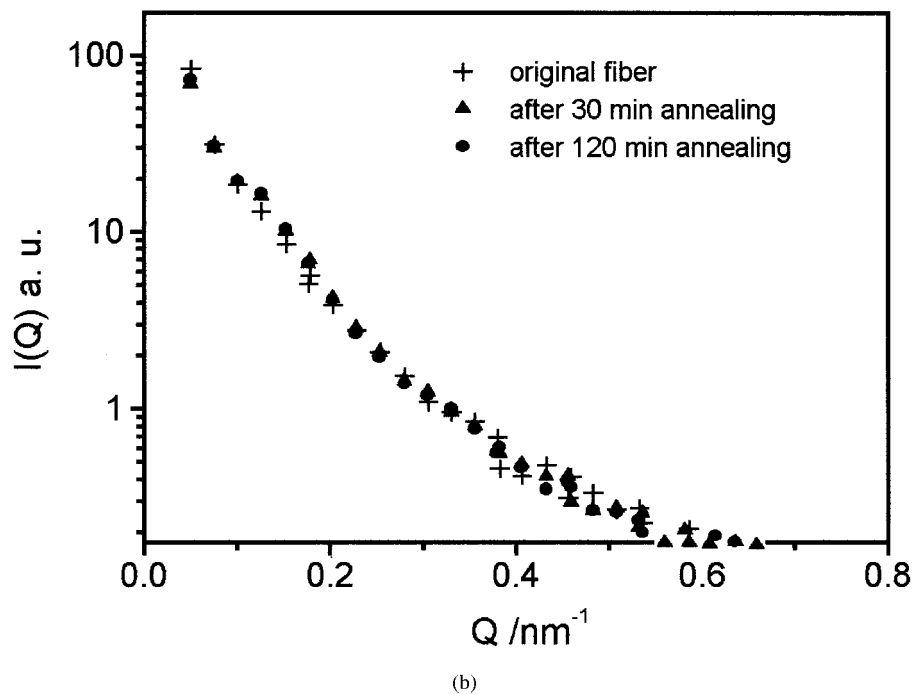
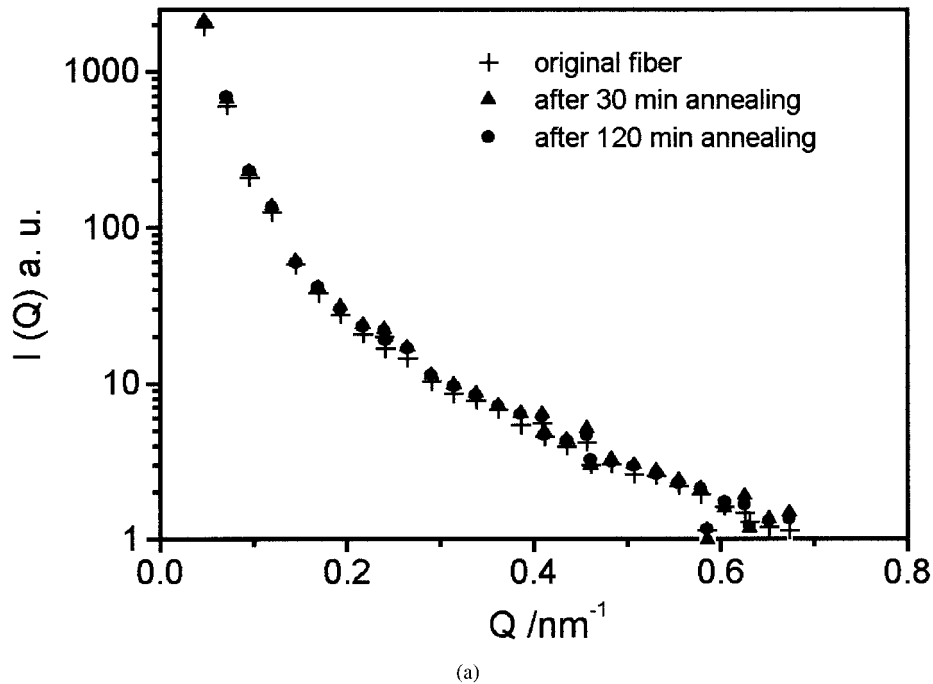


Figure 7. SAXS intensity curves taken at a 5-m scattering distance: (a) the equatorial pattern and (b) the meridional pattern.

lecular strain in the oriented intermediate phase.⁵⁶ Any melted chain segments of the orthorhombic crystals would first add to the surrounding strained intermediate phase and, therefore, have a reduced entropy of fusion that, in

turn, causes an increase in the melting temperature (superheating) until a truly amorphous phase surrounds the melting crystals.⁵⁵ The three endotherms are a measure of different states of strain in the intermediate phase and include the

transition to the hexagonal phase [see Fig. 2(a,b)].^{7,19,26} DSC after annealing at 373 K shows more melting in peak 1 of Figure 1 and lesser effects on peaks 2 and 3. This proves that on annealing strains are released in the intermediate phase, causing crystals to melt at a lower temperature.

Because the annealing behavior is expected to be irreversible, TMDSC can be used to look for reversible and irreversible thermal effects. Figure 3(a) demonstrates that differences in the thermodynamic behavior of the fibers relative to a bulk-crystallized sample reach down to the glass-transition region, centered at 237 K.⁵⁷ Up to about 405 K, the original gel-spun fiber behaves fully reversibly, as shown in Figure 3(b), despite the fact that the heat capacity has reached a value of about 60 J K⁻¹ mol⁻¹, almost double that of the vibrational heat capacity (30.7 J K⁻¹ mol⁻¹).⁴⁴ Because the overall fiber is not in thermodynamic equilibrium, we must classify the fiber as being overall metastable, but with local equilibria, which may involve volumes of only nanophase size. Expressing this latent heat exchanged per kelvin in reversible melting as orthorhombic crystallinity yields 0.7% K⁻¹. The TMDSC data agree with the picture of gel-spun fibers available to date and with the AFM results of Figure 4 and the SAXS data of Figure 7, which show no major changes occurring in the crystalline phase on annealing at 373 K.

CONCLUSIONS

The annealing of the gel-spun, ultrastrong PE fibers of ultrahigh molar mass at the low temperature of 373 K causes no detectable changes in the structure analysis by AFM and SAXS, even though considerable deterioration of mechanical properties occurs. It produces, however, a distinctly different fracture surface when the fibers are split. Instead of a brittle fracture around the constituent fibrils, a plastic deformation of the interfibrillar intermediate phase is observed. Similarly, in DSC and TMDSC experiments, one can detect no changes in the heat capacity or measurable latent heat effects in the temperature range up to the annealing temperature, which would indicate major changes in the phase structure. If we extend the analysis into the melting range, distinctly different endotherms of melting are observed after annealing that have been linked to a reduction of strain in the oriented intermediate phase on annealing. As suggested

for the ultimate strength of these fibers,¹⁷ the structure-sensitive properties are based mainly on this intermediate phase, and it is easy to generate a scenario of slackened tie molecules to account for the loss in mechanical properties. Of importance for the description of the phase structure of the fibers is the verification of the glass transition of the amorphous and intermediate phases in the temperature region up to 300 K.⁷ Finally, the detailed quasi-isothermal TMDSC analysis has proven that within the metastable, semicrystalline global network of the fibers, regions exist that can melt reversibly.

This work was supported by the Division of Materials Research of the National Science Foundation through the Polymers Program (DMR-9703692) and by the Division of Materials Sciences and Engineering of the Office of Basic Energy Sciences of the U.S. Department of Energy at Oak Ridge National Laboratory, managed and operated by UT-Battelle, LLC, for the U.S. Department of Energy under contract number DOE-AC05-00OR22725.

REFERENCES AND NOTES

1. Prevorsek, D. C.; Chin, H. B.; Murthy, S. *J Polym Sci Polym Symp* 1993, 75, 81.
2. Prevorsek, D. C. *Trends Polym Sci* 1995, 3, 4.
3. Weeden, G. C.; Tam, T. Y. *Mod Plast* 1986, 63, 64.
4. Prevorsek, D. C. In *Synthetic Fibre Materials*; Brody, H., Ed.; Polymer Science & Technology Series; Longman: London, 1994; Part 2, Chapter 10, p 264.
5. Brady, J. M.; Thomas, E. L. *Polymer* 1989, 30, 1615.
6. Furuhata, K.; Yokokawa, T.; Seoul, C.; Miyasaka, K. *J Polym Sci Part B: Polym Phys* 1986, 24, 59.
7. Kwon, Y. K.; Boller, A.; Pyda, M.; Wunderlich, B. *Polymer* 2000, 41, 6237.
8. Abo El-Maaty, M. I.; Olley, R. H.; Bassett, D. C. *J Mater Sci* 1999, 34, 1975.
9. Amornsakchai, T.; Olley, R. H.; Bassett, D. C.; Al-Hussein, M. O. M.; Unwin, A. P.; Ward, I. M. *Polymer* 2000, 41, 8291.
10. Amornsakchai, T.; Bassett, D. C.; Olley, R. H.; Unwin, A. P.; Ward, I. M. *Polymer* 2001, 42, 4117.
11. Prasad, K.; Grubb, D. *J Polym Sci Part B: Polym Phys* 1989, 27, 381.
12. Kip, B. J.; van Eijk, M. C. P.; Meier, R. J. *J Polym Sci Part B: Polym Phys* 1991, 29, 99.
13. Moonen, J. A. H. M.; Roovers, W. A. C.; Meier, R. J.; Kip, B. J. *J Polym Sci Part B: Polym Phys* 1992, 30, 361.
14. Kaji, K.; Ohta, Y.; Yasuda, H.; Murano, M. *Polym J* 1990, 22, 455.

15. Kaji, K.; Ohta, Y.; Yasuda, H.; Murano, M. *Polym J* 1990, 22, 893.
16. Chen, W.; Fu, Y.; Wunderlich, B.; Cheng, J. *J Polym Sci Part B: Polym Phys* 1994, 32, 2661.
17. Fu, Y.; Chen, W.; Pyda, M.; Londono, D.; Annis, B.; Habenschuss, A.; Cheng, J.; Wunderlich, B. *J Macromol Sci Phys* 1996, 35, 37.
18. Hu, W.-G.; Schmidt-Rohr, K. *Polymer* 2000, 41, 2979.
19. Pennings, A. J.; Zwijnenburg, A. J. *J Polym Sci Polym Phys Ed* 1979, 17, 1011.
20. Teare, P. W.; Holmes, D. R. *J Polym Sci* 1957, 24, 496.
21. Hsieh, Y.; Ju, J. *J Appl Polym Sci* 1994, 53, 347.
22. Cheng, J.; Fone, M.; Fu, Y.; Chen, W. *J Therm Anal* 1996, 47, 673.
23. Goeritz, D.; Kemmerer, J.; Kreitmeier, S.; Rossbacher, R. *Colloid Polym Sci* 1983, 261, 631.
24. Wunderlich, B.; Melillo, L. *Makromol Chem* 1968, 118, 250.
25. Hsieh, Y.; Hu, X. *J Polym Sci Part B: Polym Phys* 1997, 35, 623.
26. van Aerle, N. A. J. M.; Lemstra, P. J. *Polym J* 1988, 20, 131.
27. Kuwabara, K.; Horii, F. *Macromolecules* 1999, 32, 5600.
28. Wunderlich, B.; Möller, M.; Grebowicz, J.; Baur, H. *Conformational Motion and Disorder in Low and High Molecular Mass Crystals; Advances in Polymer Science* 87; Springer-Verlag: Berlin, 1988.
29. Tashiro, K.; Sasaki, S.; Kobayashi, M. *Macromolecules* 1996, 29, 7460.
30. Hoogsteen, W.; ten Brinke, G.; Pennings, A. J. *Colloid Polym Sci* 1988, 266, 1003.
31. Zenke, D.; Hirte, R.; Wiegand, P. *J Therm Anal* 1988, 33, 1171.
32. Boller, A.; Wunderlich, B. *J Therm Anal* 1997, 49, 343.
33. Batiaansen, C. W. M.; Lemstra, P. J. *Makromol Chem Makromol Symp* 1989, 28, 73.
34. Tsubakihara, S.; Nakamura, A.; Yasuniwa, M. *Polym J* 1996, 28, 489.
35. Arakawa, T.; Wunderlich, B. *J Polym Sci Part C: Polym Symp* 1967, 16, 653.
36. Wunderlich, B.; Czornyj, G. *Macromolecules* 1977, 10, 906.
37. Teckoe, J.; Bassett, D. C.; Olley, R. H. *Polym J* 1999, 31, 765.
38. Dijkstra, D. J.; Torfs, J. C. M.; Pennings, A. J. *Colloid Polym Sci* 1989, 267, 866.
39. Hikosaka, M. *Polymer* 1990, 31, 458.
40. Archer, D. G. *J Phys Chem Ref Data* 1993, 22, 1441.
41. Hu, W.-B.; Wunderlich, B. *J Therm Anal Calorim* 2001, 66, 677.
42. Wignall, G. D.; Lin, J. S.; Spooner, S. *J Appl Crystallogr* 1990, 23, 241.
43. Wunderlich, B.; Cormier, C. M. *J Phys Chem* 1966, 70, 1844.
44. For a description, see Wunderlich, B. *Pure Appl Chem* 1995, 67, 1919. For values, see the downloadable database at <http://web.utk.edu/~athas>.
45. Schaper, A.; Zenke, D.; Schulz, E.; Hirte, R.; Taege, M. *Phys Status Solidi A* 1989, 116, 179.
46. Wunderlich, B. *Macromolecular Physics; Academic: New York, 1974; Vol. 1.*
47. Annis, B. K.; Reffner, J. R.; Wunderlich, B. *J Polym Sci Part B: Polym Phys* 1993, 31, 93.
48. Peterlin, A. *J Mater Sci* 1971, 6, 490.
49. Peterlin, A. *Colloid Polym Sci* 1975, 253, 809.
50. Prevorsek, D. C.; Harget, P. J.; Sharma, R. K.; Reimschuessel, A. C. *J Macromol Sci Phys* 1973, 8, 127.
51. Wunderlich, B.; Melillo, L.; Cormier, C. M.; Davidson, T.; Snyder, G. *J Macromol Sci Phys* 1967, 1, 485.
52. Peterlin, A. *J Appl Phys* 1977, 48, 4099.
53. Hoogsteen, W.; Pennings, A. J.; ten Brinke, G. *Colloid Polym Sci* 1990, 268, 245.
54. Grubb, D. T.; Prasad, K. *Macromolecules* 1992, 25, 4575.
55. Wunderlich, B. *Macromolecular Physics; Academic: New York, 1980; Vol. 3.*
56. Wunderlich, B.; Boller, A.; Okazaki, I.; Ishikiriya, K.; Chen, W.; Pyda, M.; Pak, J.; Moon, I.; Androsch, R. *Thermochim Acta* 1999, 330, 21.
57. Gaur, U.; Wunderlich, B. *Macromolecules* 1980, 13, 445.